Journal of Biomedical Optics

SPIEDigitalLibrary.org/jbo

Dissecting eukaryotic cells by coherent phase microscopy: quantitative analysis of quiescent and activated *T* lymphocytes

Vladimir P. Tychinsky
Alexander V. Kretushev
Tatiana V. Vyshenskaya
Alexander A. Shtil

SPIE

Dissecting eukaryotic cells by coherent phase microscopy: quantitative analysis of quiescent and activated *T* lymphocytes

Vladimir P. Tychinsky,[a] Alexander V. Kretushev,[a] Tatiana V. Vyshenskaya,[b] and Alexander A. Shtil[c]
[a]Moscow Institute of Radioengineering, Electronics and Automation, Laboratory of Coherent Phase Microscopy, 78 Vernadsky Avenue, Moscow 119454, Russia
[b]Moscow State University, Department of Physics, Vorob'evy Gory, Moscow 119992, Russia
[c]Blokhin Cancer Center, 24 Kashirskoye Shosse, Moscow 115478, Russia

Abstract. We present a concept for quantitative characterization of a functional state of an individual eukaryotic cell based on interference imaging. The informative parameters of the phase images of quiescent and mitogen-activated *T* lymphocytes included the phase thickness, phase volume, the area, and the size of organelles. These parameters were obtained without a special hypothesis about cell structure. Combinations of these parameters generated a "phase portrait" of the cell. A simplified spherical multilayer optic model of a *T* lymphocyte was used to calculate the refractivity profile, to identify structural elements of the image with the organelles, and to interpret the parameters of the phase portrait. The values of phase image parameters underwent characteristic changes in the course of mitogenic stimulation of *T* cells; thereby, the functional state of individual cells can be described using these parameters. Because the values of the components of the phase portrait are measured in absolute units, it is possible to compare the parameters of images obtained with different interference microscopes. Thus, the analysis of phase portraits provides a new and perspective approach for quantitative, real-time analysis of subcellular structure and physiologic state of an individual cell. © *2012 Society of Photo-Optical Instrumentation Engineers (SPIE).* [DOI: 10.1117/1.JBO.17.7.076020]

Keywords: coherent phase microscopy; subcellular structures; optical model of living cell; T lymphocyte; phytohemagglutinin.

Paper 12197 received Mar. 27, 2012; revised manuscript received May 23, 2012; accepted for publication Jun. 18, 2012; published online Jul. 17, 2012.

1 Introduction

In recent years, the interest emerged in the development of new optical methods for individual cell analysis. A significant progress took place in interference methods for evaluation of red blood cells.[1–5] These techniques allow for highly accurate measurement of critical parameters of the cell, that is, the refractive index, the geometric volume, and the spectrum of fluctuations. In particular, the refractive index (or refractivity, i.e., the difference between the refractive indices of the object and the environment) is one of the most informative parameters of an individual cell.[1–5] Its diagnostic importance has been demonstrated by characteristic changes of erythrocytes infected with *Plasmodium falciparum*.[2,3] The approaches based on holography,[4,5] phase contrast, and common-paths method[6] have been applied to measure the refractive index by interference microscopy. In so doing, a variety of algorithms, models,[1–10] and several methods of image recording can be combined in a single instrument. The method of spatial interference microscopy (SLIM-fluorescence multimodal imaging) developed by Popescu and colleagues[11] allows for simultaneous recording of structural elements and dynamic processes in neurons.

Common for all interference methods is the representation of the images in the form of a 2-D distribution $h(x, y)$ of optical path difference (OPD) in the image plane. The most important and the unique advantage of the interference microscopy is the measurement of OPD in absolute units of wavelength[1–11] with very high precision, which is hardly achievable or impossible with other methods. In addition, the common-path method allowed to significantly decrease the sensitivity of images to external acoustic noise.[8] Modern models of interference microscopes allow for measuring OPD based on various modulation methods and algorithms.[3–5,8,9] In particular, the measurements were made with a raster OPD-compensation method providing a significant improvement of resolution.[9,12,13]

Most studies using interference microscopy have been performed with red blood cells,[1–5] whereas other biological objects have been seldom addressed.[7,10–12] One reason for this preference might be optical homogeneity of erythrocytes. Because these cells lack optically contrast elements, e.g., the nuclei and organelles, erythrocytes may be well characterized by mean refractive index.[1–5] However, the mean volume-averaged refractivity is insufficient for characterization of optically heterogeneous mononuclear cells, such as *T* lymphocytes. A significantly more complex algorithm and much higher spatial resolution are required for the analysis of intracellular structures. Furthermore, a problem arises as to how to interpret the phase images of the optically complex object. These issues have been discussed with respect to the refractivity of single mitochondria, chloroplasts, cyanobacteria, and human cells by coherent phase microscopy.[7,9,10,12]

Address all correspondence to: V. P. Tychinsky, Moscow Institute of Radioengineering, Electronics, and Automation, Laboratory of Coherent Phase Microscopy, 78 Vernadsky Avenue, Moscow 119454, Russia. Tel: 7495-434-6792; Fax: 7495-434-8665; E-mail: vtych@yandex.ru

0091-3286/2012/$25.00 © 2012 SPIE

In this study, we propose an approach to characterize an individual cell, namely the T lymphocyte, by its phase portrait, which is a set of physical parameters of subcellular structures. We believe that such a portrait can be supplemented by data obtained with other methods and serve for evaluation of the physiologic state of the cell.

2 Experimental Details

Measurements were performed on a microscope Airyscan.[7,9,12,13] The cells were illuminated with a collimated beam of light. In the phase images no speckles were observed, in spite of relatively big coherence length of the He-Ne laser ($\lambda =$ 633 nm, 1 mW) used for illumination. The OPD values were determined sequentially in each pixel of the phase image by the compensation method. The phase of the reference wave varied linearly and periodically with a movable mirror in the reference arm of the interferometer. The image raster-scanning was performed by a coordinate sensitive photodetector, that is, the dissector image tube LI-620. This method allowed us to get super-diffraction spatial resolution,[9,13] and to record cellular processes in real-time.[12] The sensitivity to OPD changes limited by noise was ~1 nm; therefore, the characteristics of the interference microscope did not seriously limit the results of measurements.

The suspension of T-lymphocytes isolated from peripheral blood of healthy donors was provided by I. Vasilenko (Moscow Institute of Clinical Research). Freshly isolated cells were resuspended in medium 199 (Sigma-Aldruch) supplemented with 5% fetal calf serum (HyClone) and incubated at 37°C for 1 h without (quiescence) or with 2 μg/mL phytohemagglutinin (PHA; Sigma-Aldrich activation). To prepare the sample for the analysis, a drop of the cell suspension was applied on a polished silicon wafer, covered with a cover slip, and placed on a table of the coherent phase microscope Airyscan. The position of the sample in the chamber is shown schematically in Fig. 1(a). A 15-μm-thick spacer between the silicon substrate and the cover slip prevented cell deformation. Measurements of each sample were conducted within 20 min. A removable screen was used to minimize the effect of laser radiation on cells. Fifty individual cells were analyzed per each sample.

3 Results and Discussion

3.1 *Concept of Zones and Characteristic Parameters in the Phase Image of the Cell*

Normally, the phase image is described as the function:[7–9]

$$h(x,y) = \int [n(x,y,z) - n_e]\mathrm{d}z, \tag{1}$$

in the image plane (x,y), where $n(x,y,z)$ and n_e are the refractive indices of the object and the environment, respectively. The function $h(x,y)$ can be interpreted as a "projection" of the refractive index onto the image plane. Under certain conditions, the inverse problem can be solved when the function $n(x,y,z)$ is restored from its projection.[1–6,14]

A fundamentally different approach involves the determination of the characteristic parameters of the function $h(x,y)$. We analyzed this approach using a model of an optically heterogeneous object represented by a system of concentric spherical layers with the diameters d_i, volumes $V_i = \pi[(d_i)^2 - (d_{i+1})^2]/4$, and the refractive indices n_i. The section of such an object by the vertical plane (x,z) is shown in Fig. 1(a). For example, OPD h_2 in the point d_2 is the sum of contribution of two layers: $h_2 = H_{20}\Delta n_0 + H_{21}\Delta n_1$, where in the geometric path H_{ji} the first index "j" corresponds to the position of the point, and the second index "i" corresponds to the number of the layer. In general, the value of OPD at the boundary of j'th zones can be represented as the sum:

$$h_j = \Sigma H_{ji}\Delta n_i, \tag{2}$$

where $\Delta n_i = n_i - n_e$ is its refractivity. For example, at the border of the $3d$ zone ($j = 3,\ 1 \le i \le 3$), $h_3 = H_{30}\Delta n_0 + H_{31}\Delta n_1 + H_{32}\Delta n_2$.

The OPD "jumps" in the image plane (x,y) in the proximity of the points that are the projections of the adjacent layer due to the difference $(\Delta n_3 - \Delta n_2)$. The projections of the boundaries of these layers in the topogram [Fig. 1(b)] are represented by concentric circles. The area delimited by the circles with the diameters d_i and d_{i+1}, is called henceforth the i'th zone; the change of OPD within a zone is assumed to be smooth, that is, without abrupt changes. The number of the zone corresponds to the index of the external ring diameter.

The null zone is bound by the diameters (d_0, d_1); its area $\Delta S_{01} = S(h_0) - S(h_1)$. The algorithm for determining the boundaries will be discussed in Sec. 3. The boundaries of the zones are represented by the circles, even though they generally form a closed contour $h_i(x,y) = \mathrm{const}$ [Fig. 1(b), dotted]. Figure 1(c) presents two phase thickness profiles $h(x)$ and $h(y)$ in the orthogonal cross-sections of the topogram. The points with characteristic values of the phase thickness (h_i) and diameter (d_i) corresponding to the boundaries of the zones are depicted in one of the profiles.

Our concept can be summarized as follows:

(1) A limited number of borders of zones $h_i(x,y) = \mathrm{const}$ can be determined in the phase image of an optically heterogeneous object (e.g., a nucleated cell). The algorithms for determining the boundaries for the function $h(x,y)$ and for the phase thickness profile are assumed to be known.

(2) Certain characteristic parameters of the function $h(x,y)$ can be determined within the zones and at their boundaries. The system of these parameters in their entirety (phase portrait) reflects the morphology and physiologic state of the cell.

(3) It is possible to estimate the key parameters of the function $h(x,y)$: the phase thickness, the area and the equivalent diameter of the zones, and the phase volume of the zone. The optical models of the cell are necessary to determine other parameters such as refractivity and geometric volume of organelles.

(4) Biophysical interpretation of the parameters of the phase portrait can be performed if information about the structure and the dimensions of the organelles is available [Fig. 1(d)].

In line with this concept, we used the following functions and parameters of the phase image of an individual T lymphocyte:

(a) Phase thickness profiles $h(x, y = \mathrm{const})$, $h(y = \mathrm{const}, x)$, i.e., the relationship between the phase

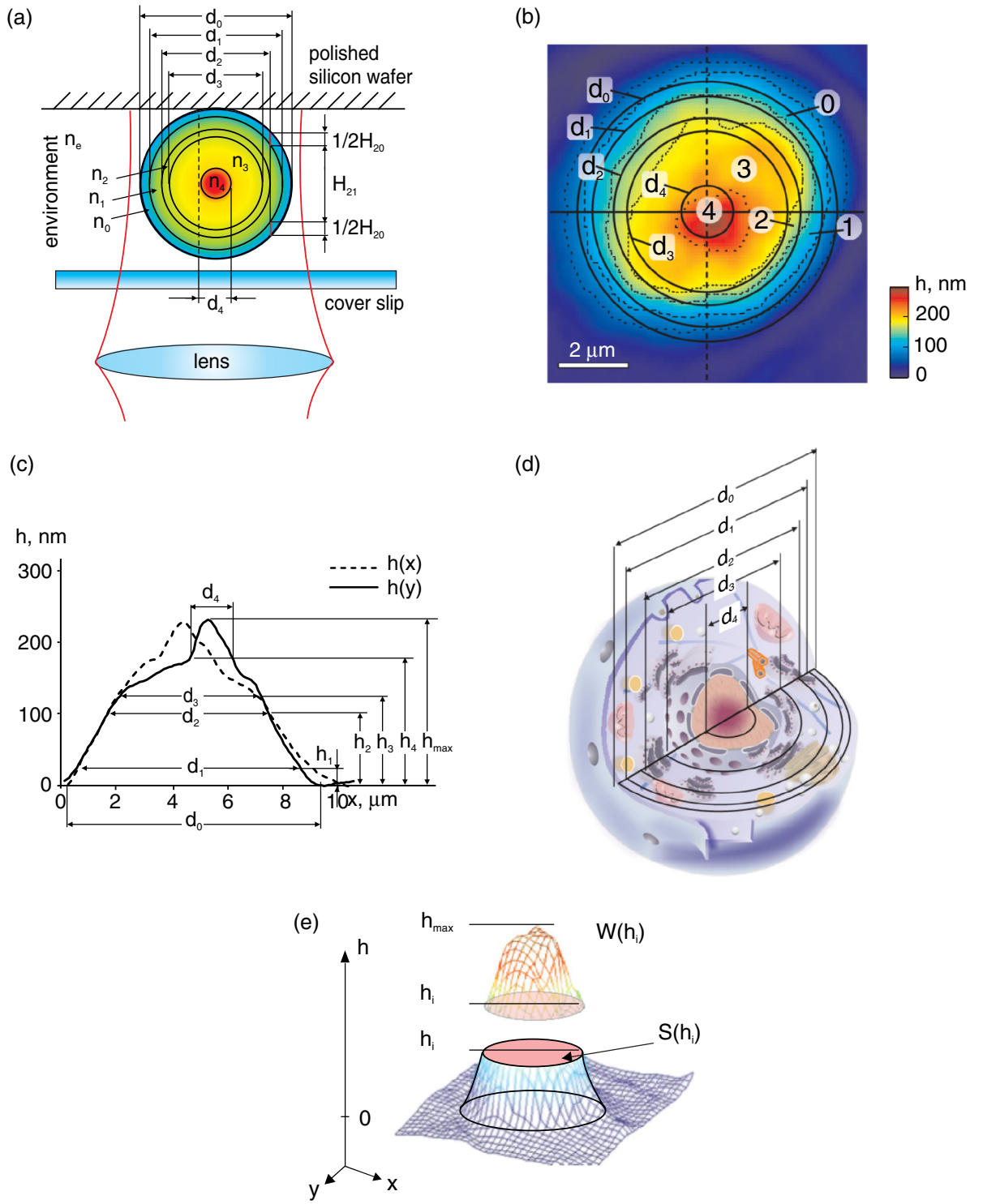

Fig. 1 The concept of zones and meaningful parameters in the phase image of *T* lymphocytes. (a) Schematic representation of an optically heterogeneous cell in the chamber as a set of spherical layers of different diameters and refractive indices. (b) The projection of the boundary of the *i*'th spherical layer with the diameter d_i is marked in the topogram $h(x, y)$ or a phase image of a *T*-lymphocyte. The diameter d_0 corresponds to the outer boundary of the cell. Numbers refer to the zones: 0, the peripheral part of the cytoplasm; 1, dense part of the cytoplasm; 2, chondriome, a giant branched mitochondrion; 3, nucleus; and 4, nucleolus. In general, the boundaries of the zone can be represented by dotted contours of $h_i(x, y) = \text{const}$. The area $S(h_i) = \pi(d_i)^2/4$ surrounded by a contour $h_i(x, y)$, was used to calculate the diameter (d_i) of the circle with the equivalent area. (c) Profiles of the phase thickness $h(x)$ and $h(y)$ in orthogonal sections of the *T*-lymphocyte topogram $h(x, y)$ differ due to the asymmetry of the structures. In the characteristic points of the profile $h(x)$ the diameters d_i and the phase thickness values $h_i (i = 1 - 4)$ are marked that coincide with the positions of characteristic points in the graphs of functions $S(h_i)$ and $W(h_i)$. Parameters at the boundaries of the zones were determined in the points of characteristic values h_i. h_{max} is maximum value of the phase thickness. (d) Adequate interpretation of the cell phase image requires information about the dimensions of subcellular structures. The cytoplasm, the chondriome, the nucleus, and the nucleolus are presented as spherical regions with different diameters. (e) A 3-D image $h(x, y)$ of *T* lymphocyte includes a fragment bounded by h_{max} and the horizontal plane $h_i = \text{const}$, the phase volume of $W(h_i)$, and the cross-section area $S(h_i)$.

thickness and the coordinate, e.g., in the orthogonal diametrical sections of the topogram $h(x, y)$.

(b) Characteristic values of the phase thickness (h_i) at the boundaries of zones.

(c) Area-equivalent diameters (d_i) of the circles at the boundaries of the zones.

(d) The function $S(h)$, i.e., the relationship between the area within the contour $h(x, y) = \text{const}$ in the horizontal planar cross-section and the phase thickness h [Fig. 1(e)].

(e) The area $S(h_i)$ delimited by the i'th boundary and the area of the i'th zone $\Delta S_{i,i+1}$.

(f) The function $W(h)$, i.e., the relationship between the phase volume of the cell in the interval [0; h] and the phase thickness [Fig. 1(e)].

(g) Phase volume $W(h_i)$ delimited by the i'th boundary and the phase volume of the i'th zone $\Delta W_{i,i+1} = W(h_i) - W(h_{i+1})$.

(h) The values of refractivity at the boundaries of zones (Δn_i) and within the zones ($\langle \Delta n_i \rangle$).

(i) Refractivity profiles $\Delta n(r)$.

(j) The cytoplasmic area index $I_S = \Delta S_{23} + \Delta S_{34} + S_4)/S_0$, the geometric volume index $I_V = (\Delta V_{23} + \Delta V_{34} + V_4)/V_0$, and the phase volume index $I_W = (\Delta W_{23} + \Delta W_{34} + W_4)/W_0$.

The phase volume W_0 of the whole cell is the sum of all segments of the phase volumes $W_0 = \Sigma \Delta n_i V_i$, where V_i is geometric volume of the i'th organelle. A part of the phase volume $W(h_i)$ of the cell limited by the horizontal plane $h_i = \text{const}$ and the area $S(h_i)$ in the section of a 3-D image of T lymphocyte are shown in Fig. 1(e). A more detailed explanation of these functions and parameters is given in Secs. 3.3 and 3.4. Of note, no cell model, or a priori information about cell structure are needed to determine these parameters, except those mentioned in the items h, i, and j.

The algorithm for determining the zone boundaries based on the phase thicknesses values (h_i) is important, because their accuracy significantly affects the parameters of the phase portrait. The criterion for the zone boundaries in the phase image of the cell is local change in the slope of the phase thickness profile $h(x)$, $h(y)$ and/or the patterns of $S(h)$ and $W(h)$ (Sec. 3). This algorithm is based on the assertion that the boundary between the zones coincides with the projection of the abrupt change of the refractive index onto the image plane in the optically heterogeneous object. An alternative definition of the zone boundaries can be obtained from the refractivity profile function $\Delta n(r)$. However, the necessity to use an optical model seems to be disadvantageous.

Several indices were used to determine the boundaries between the zones and their parameters. These indices were provisionally identified with organelles using the notation for the phase thickness profile [Fig. 1(c)]: 0 for the outer boundary of the cell; 1. for the border between the peripheral and dense parts of the cytoplasm; 2. for the boundary of the dense cytoplasm with the chondriome, the giant branched mitochondria; 3. for the border between the chondriome and the nucleus; and 4. for the border between the nucleus and the nucleolus. It is noteworthy that the boundaries of organelles in phase images may or may not coincide with the respective boundaries obtained by other optical methods. The values of the area at the border of the i'th zone $S(h_i)$ were used to calculate the area-equivalent diameter (d_i) of the circles instead of the contour $h_i(x, y) = \text{const}$. The diameters (d_i) of the circles are shown in the topogram [Fig. 1(b)] and in the phase thickness profile [Fig. 1(c)].

An optical model of the cell is required to determine the zones and to calculate the refractivity (Δn_i) at their boundaries. The phase thickness at the i'th boundary of the profile $h(x_i) = h_i$ in this model can be represented as a summed contribution of the refractivity and the geometric thickness of the layers according to Eq. (2). The solution of the system of Eq. (2) gives the values of refractivity Δn_i of the layers. Note that there is no need to define the boundaries of the zones to calculate the refractivity profile $\Delta n(r)$ in the multilayered spherical model.[14]

We present the measurements of T lymphocytes isolated from peripheral blood of healthy donors. Measurements were performed with a coherent phase microscope Airyscan developed by us. Its design and parameters have been described in detail elsewhere.[7,9,10,12].

3.2 *Phase Portrait of a Quiescent T lymphocyte*

The points in phase thickness profiles $h(x)$ and $h(y)$ obtained in the orthogonal diametrical sections of the topogram include the diameters (d_i) and the thicknesses (h_i) that we identified with the boundaries of zones. As shown in Fig. 1(c), the shapes of the phase thickness profiles $h(x)$ and $h(y)$ slightly differ, probably due to certain deviation of the internal structure from perfect central symmetry.

The profile $h(x)$ can be interpreted as follows. The zero level of the phase thickness ($h_0 = 0$) [Fig. 1(c)] corresponding to the equivalent circle of diameter d_0, defines the outer boundary of the cell. As follows from the comparison of Fig. 1(b)–1(c), only a peripheral part of the cytoplasm corresponding to the zone 0 significantly contributes to the phase thickness within the interval $0 \le h \le h_1$. The phase thickness tends to increase toward the cell center as determined by continuously increased contribution of subcellular structures: the boundaries of the zone 1 correspond to thicknesses $h_1 - h_2$ and diameters $d_1 - d_2$. It is reasonable to suppose that the increase of the phase thickness from h_1 to h_2 is due to the contribution of the layer 1 whose refractivity (Δn_1) is quite high. The latter parameter was stable; we identified the layer 1 as the "dense" part of the cytoplasm. The increase of the phase thickness in the zone 2 ($h_2 - h_3$) is associated with an additional contribution of the chondriome, in the 3d zone ($h_3 - h_4$) with contribution of the nucleus, and in the 4th zone ($h_4 \le h \le h_{\max}$), with the nucleolus.

The position of characteristic points in the profiles $h(x)$ and $h(y)$ depends on the symmetry of the structure, the location of the section and is not necessarily single-valued. More reproducible values of h_i can be obtained from the statistical portrait of the topogram [Fig. 1(b)], e.g., from the graph $S(h)$ [Fig. 2(a)]. A slow increase in the phase thickness at the boundary of the cell in a range $0 \le h \le h_1$ [Fig. 1(c)] corresponds to the area

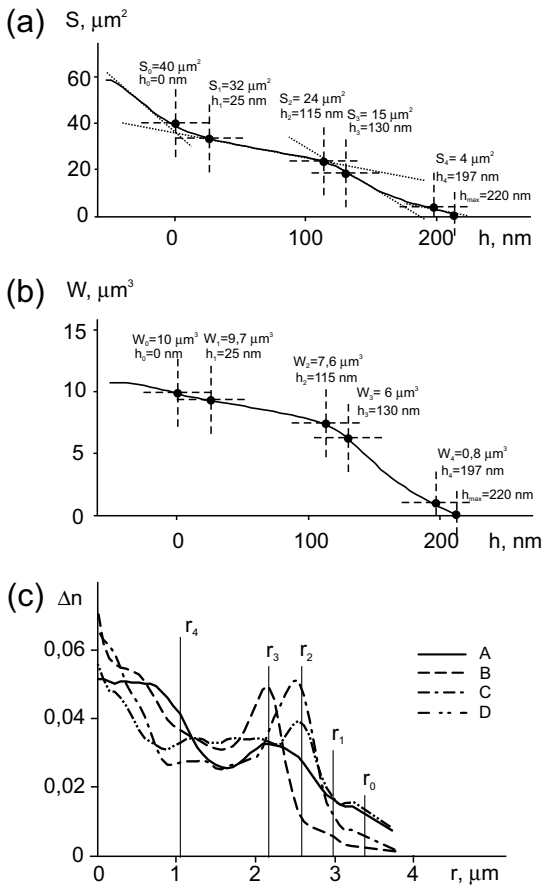

Fig. 2 Parameters of a quiescent T lymphocyte. (a) The function $S(h)$, shows the dependence of the cross-section area on the phase thickness (h). Its value increases toward the periphery of the T lymphocyte. We adopted the left point of the intersection of tangents as the zero point for phase thickness ($h = 0$). This point corresponds to the entire cell surface $S_0 = 40\ \mu m^2$. At the border of the nucleolus ($h_4 \approx 200$ nm) the surface is $S_4 \leq 4\ \mu m^2$. The position of other characteristic points identified with the boundaries between the zones is defined by the intersection ($h_2 = 115$ nm; $h_3 = 130$ nm) or at the point of contact ($h_1 \approx 25$ nm). The area $S(h_i)$ inside the boundaries of the i'th zone is used to determine the diameter (d_i) of the equivalent circle. (b) The characteristic points of the phase volume $W(h)$ and area $S(h)$ functions coincide. The values of $W(h_i)$ at the boundaries between the zones were used to estimate the phase volumes of layers. (c) Profiles of the phase thickness $h_{A-D}(r)$ are the functions of the distance (r) from the cell center along the radii that differ by rotation on 90°. The difference can be explained by asymmetry of subcellular structures. The values of radii r_i identified with the boundaries of organelles are marked with indices $i = 1 - 4$. Relatively flat parts of the refractivity profile ($\Delta n_3 = 0.03 \div 0.035$) in the interval $r = 0.7 \div 2.0\ \mu$m correspond to the nucleus; the interval nearest to the center ($r \leq 0,8\ \mu$m) with $\Delta n_4 = 0.05 \div 0.065$ is attributed to the nucleolus.

difference $S_0 - S_1$ [Fig. 2(a)]. It reflects the contribution of the refractivity (Δn_0) of the zone 0 attributed to the peripheral area of the cytoplasm.

The point $h = 0$ corresponds to a change of the $S(h)$ function slope. Its position can be determined more accurately from the intersection of tangents of the adjacent parts of $S(h)$ [Fig. 2(a)]. The ordinate at the intersection of the tangents [$S_0 = S(h = 0) = \pi(d_0/2)^2 = 40\ \mu m^2$] represents the number of pixels in the cell image. This gives the value of the entire cell area and allows to calculate the diameter $d_0 = 7.14\ \mu$m of an equivalent circle area. The position of the next characteristic point (h_1), which can be regarded as the inner boundary of the zone 0 separating the periphery and a "dense" part of the cytoplasm, can be identified by the point of changed slope ($h_1 \approx 25$ nm) in the phase thickness profile [Fig. 1(c)]. The position of this point can be obtained with even higher accuracy from the graph of $S(h)$ function, assuming that the boundary criterion is based on the location of the characteristic point h_1. The ordinate $S(h_1) = S_1 = 32\ \mu m^2$, the diameter of the circle $d_1 = 6.38\ \mu$m, and the geometric volume $V_1 = \pi(d_1)^3/6$ were accepted as the characteristics of the boundary of the zone 1. Apparently, the accuracy of the zone boundaries determined by this method should depend on the difference in the slope tangents on both sides of the characteristic points. Given that the refractivity changes monotonously and the optical homogeneity of the cell increases, the boundary between the zones may become less contrast and finally disappear.

The values of the phase thicknesses, the area, the diameter, and the volume of geometric layers at the boundaries of corresponding zones were: $S_0 = 40\ \mu m^2$, $d_0 = 7.15\ \mu$m, $\Delta V_{01} = 54\ \mu m^3$; $S_1 = 32\ \mu m^2$, $h_1 \approx 25$ nm, $d_1 = 6.4\ \mu$m, $\Delta V_{12} = 49\ \mu m^3$; $S_2 = 24\ \mu m^2$, $h_2 = 115$ nm, $d_2 = 5.5\ \mu$m; $S_3 = 15\ \mu m^2$, $h_3 = 130$ nm, $\Delta V_{23} = 43\ \mu m^3$; $d_3 \approx 3.6\ \mu$m, $\Delta V_{34} = 42\ \mu m^3$; $S_4 \approx 4\ \mu m^2$, $h_4 = 197$ nm, $d_4 \approx 1.6\ \mu$m, $\Delta V_4 = 2\ \mu m^3$, $h_{max} = 220$ nm. The areas of the zones (rings) were determined as the difference in the area values at boards, μm^2: $\Delta S_{01} = S_0 - S_1 = 8$ (zone 0); $\Delta S_{12} = 8$ (zone 1); $\Delta S_{23} = 14$ (zone 2); $\Delta S_{34} = 11$ (zone 3); $\Delta S_{45} = S_4 \approx 4$ (zone 4).

The dependence of the phase volume $W(h)$ on the phase thickness for a quiescent T lymphocyte is shown in Fig. 2(b). The values of the phase volume $W(h_i)$ at the boundaries of the zones were 10 μm^3; 9.7 μm^3; 7.6 μm^3; 6.0 μm^3; and 0.8 μm^3, respectively. The characteristic points in the $W(h)$ and $S(h)$ graphs coincided, the algorithms for its determination were also identical. The dense part of the T lymphocyte (zones 3–5, $\Delta S_{23} + \Delta S_{34} + S_4 = 29\ \mu m^2$) was $\sim I_S \approx 75\%$ of the total area ($S_0 = 40\ \mu m^2$). Accordingly, for the geometric volume of the whole cell $V_0 = 190\ \mu m^3$, the index $I_V = 49\%$; for the phase volume $W_0 = 10\ \mu m^3$, the index $I_W = 76\%$. These values correspond to the nucleus-to-cytoplasm ratio frequently used as a quantitative parameter in cell morphology.

Comparison of the parts of the phase thickness profile in Fig. 1(c) with the values of the characteristic points in Fig. 2(a) suggests the following interpretation of the zones in the topogram [Fig. 1(b)]. Only a peripheral part of the cytoplasm projects and contributes to the phase thickness of the zone 0 with the area $\Delta S_{01} = S_0 - S_1 = 8\ \mu m^2$ limited by the external ($d_0 \approx 7.14\ \mu$m, $h_0 = 0$) and internal ($d_1 \approx 6.4\ \mu$m, $h_1 = 25$ nm) circles. The part of the cell corresponding to a larger slope in the profile $h(x)$ and a higher optical density, is projected onto the area of the 1st zone $\Delta S_{12} = S_1 - S_2 = 8\ \mu m^2$. As noted above, the zone 1 is primarily attributed to the dense part of the cytoplasm whereas the peripheral part contributes to its phase thickness insignificantly. The parts (organelles) with the total phase thickness within the range $0 \leq h \leq h_3 = 130$ nm provide additive contributions to the zone 2. Finally, the areas of the zones 3 and 4 correspond to the interval $130\ \text{nm} \leq h \leq h_{max} = 220$ nm.

The values of the characteristic points of $W(h)$ function [Fig. 2(b)] also represent important parameters of the phase portrait and provide valuable information about the morphology of T lymphocytes. A low steepness $S(h)$ in the range $0 \leq h \leq 115$ nm reflects a weak refractivity of the cytoplasm. A higher

steepness $S(h)$ within 115 nm $\leq h \leq$ 130 nm may account for a higher refractivity and large geometric volume of the dense structures such as the chondriome and the nucleus. Figure 2(b) presents the values of the phase volumes $W(h_i)$ at the boundaries of the zones. Accordingly, the difference in these values allows for estimation of the phase volumes of the structures projected onto these zones, μm^3: $\Delta W_{01} = 0.3$; $\Delta W_{12} = 2.1$; $\Delta W_{23} = 1.6$; $\Delta W_{34} \approx 5.2$; $\Delta W_{45} = W_4 \approx 0.8$. An average value of the refractivity $\langle \Delta n_{01} \rangle = \Delta W_{01}/V_{01} \approx 0.0055$ can be obtained from the geometrical volume $V_{01} \approx 54\ \mu m^3$ of the peripheral cytoplasm. These values of the phase volumes could provide indirect estimates of the refractivity of organelles. However, their values depend on the accuracy with which the geometric volume is determined in the optical model of the cell. In Sec. 3.3 we show that more reasonable values of refractivity can be obtained by solving the system of Eq. (2).

3.3 *Refractivity of Organelles*

The profiles of refractivity $\Delta(_r)$AD in the cross-sections *A*-*D*, calculated with the algorithm presented in Ref. 14 are shown in Fig. 2(c). The difference in the shape and position of the maxima of orthogonal sections *A*-*D* made in orthogonal directions is probably a consequence of deviation from central symmetry of the optical density distribution of the *T* lymphocyte. Spatial heterogeneity of the structure of the chondriome can be observed by electron[15–17] and fluorescence microscopy. The radii $r_i = d_i/2$ in Fig. 2(c) approximately correspond to the zone borders in Fig. 1(b). The interval of radii $r_0 - r_1 \approx 3.7 - 3.2\ \mu m$ and a low refractivity $\langle \Delta n_{01} \rangle \approx 0.005 - 0.008$ should be identified with the zone 0 and the peripheral cytoplasm. The next interval ($r_1 - r_2 \approx 3.2 - 2.7\ \mu m$, $\langle \Delta n_{12} \rangle \approx 0.01 - 0.015$) can be identified with the dense part of the cytoplasm, whereas the interval ($r_2 - r_3 \approx 2.7 - 2.2\ \mu m$, $\langle \Delta n_{23} \rangle \approx 0.035 - 0.05$) can be identified with the chondriome. In our experiments rotenone, a drug that blocks mitochondrial respiration, caused a marked decrease of refractivity.[7,10] Similar changes in the zone 3 can also occur in mitogen-activated *T* cells (see Sec. 3.4). Finally, the zone corresponding to the next interval ($r_3 - r_4 \approx 2.2 - 0.8\ \mu m$, $\langle \Delta n_{34} \rangle \approx 0.03$) can be identified as the nucleus, and the interval ($0 - r_4 \approx 0 - 0.8\ \mu m$, $\langle \Delta n_{34} \rangle \approx 0.05 - 0.055$) with the nucleolus.

These values of refractivity, together with previously determined geometrical volumes of the layers, allow for the estimation of the phase volume of the layers. Thus, it becomes possible to determine a variety of parameters in the phase image of an individual cell. Some of these parameters [$h_i, W(h_i), S(h_i), \Delta V_{i,i+1}, I_S, I_V, I_W$] do not depend on the assumptions about the cell shape and other details of the optical model. However, the values of the zone refractivity and the refractivity profiles do depend on the adequacy of the optical model for the concrete cell. Therefore, the refractivity of organelles is probably less reliable because this parameter depends on the adequacy of a multilayered model and deviations from the spherical symmetry.

Table 1 shows the parameters of the phase portrait of an intact *T* lymphocyte. The values ΔS, ΔW, and $\langle \Delta n_i \rangle$ correspond to the zones, not to the zone boundaries. The variability of the parameters calculated after measurements of up to 50 individual cells was relatively small. Commonly the following limits were determined: maximum phase thickness $h_0 = 200 \div 250$ nm, the area $S_0 = 40 \div 50\ \mu m^2$, the phase volume $W_0 = 8 \div 12\ \mu m^3$, and mean values of whole cell refractivity $\langle \Delta n \rangle = 0.03 \div 0.04$. The variability of other parameters tended to stay within the same limits.

3.4 *Phase Portrait of the Mitogen-Stimulated T lymphocyte*

The plant mitogen PHA is known to be a polyclonal activator of *T* lymphocytes.[15–17] In the initial period of activation (within $\approx$ 1 h of exposure) PHA stimulates a transition from the "resting" phase G_0 into G_1. One may expect that the processes in PHA-activated *T* lymphocyte can be manifested in the phase images (Fig. 3). The phase thickness significantly decreased (from 220 nm to $\approx$150 nm) after 1 h with 2 μg/mL PHA. The shape of the phase thickness profile of the *T* lymphocyte changed [Fig. 3(a)]. The profile became more flat, its outer diameter increased up to $d_0 \approx 9.8\ \mu m$ mainly due to the peripheral areas of the cytoplasm. These changes involved an increase of both the entire cell area to $S_0 = 75\ \mu m^2$ and the proportion of the peripheral cytoplasm ($\Delta S_{01} = 32\ \mu m^2$), which is clear from the

Table 1 Phase portrait of a quiescent *T* lymphocyte.

Parameter, boundary	0	1	2	3	4	h_{max}
h_i, (nm)	0	25	115	130	197	220
d_i, (μm)	7.15	6.4	5.5	3.6	1.6	–
S_i, (μm^2)	40	32	24	15	4	–
W_i, (μm^3)	10	9.7	7.6	6	0.8	–
$\Delta S_{i,i+1}$, (μm^2)	8	8	9	11	4	–
$\Delta W_{i,i+1}$, (μm^3)	0.3	2.1	1.6	5.2	0.8	–
$\langle \Delta n_i \rangle$	0.004	0.015	0.044	0.035	0.05	–
$\Delta V_{i,i+1}$ (μm^3)	54	49	43	42	2	–

Note: Here and in Table 2 shown are mean values of measurements of 50 cells per each sample. Standard deviations were within 10%.

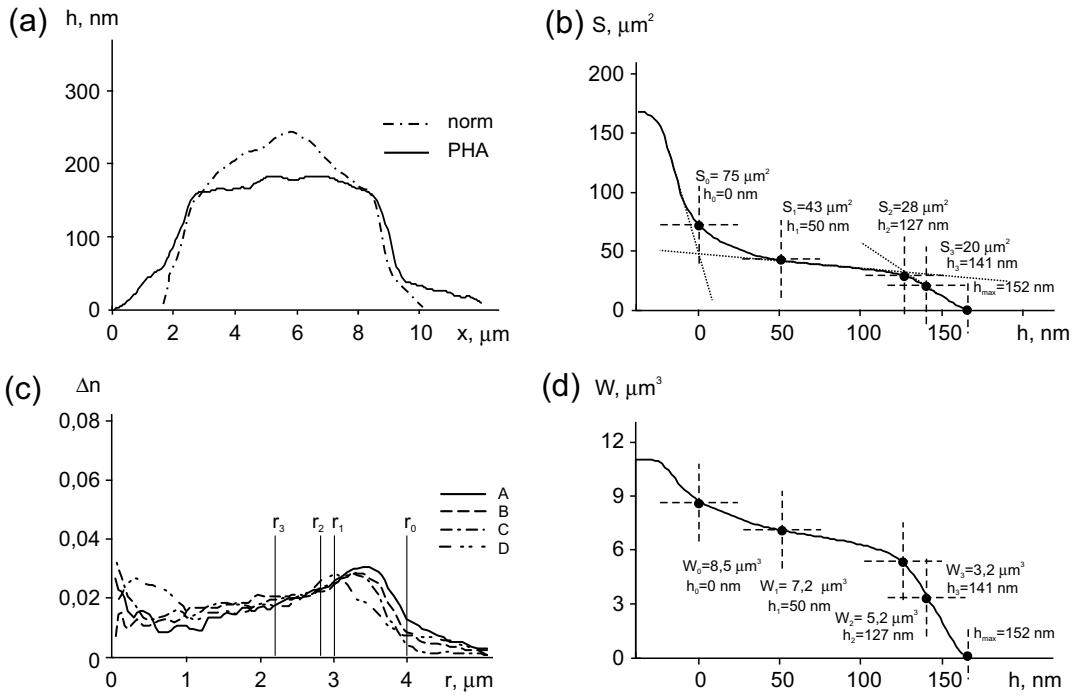

Fig. 3 Parameters of a PHA-activated *T* lymphocyte. (a) A decreased phase thickness profile and a change of overall shape compared to the quiescent cell. (b) The area of the cell $S_0 \approx 75\ \mu m^2$ increased at the expense of regions with low phase thickness ($h \leq 60$ nm). (c) Comparison with Fig. 3(a) shows that the position of characteristic points of $W(h)$ and $S(h)$ functions are the same. In PHA-treated cells the function $W(h)$ shows a 4-fold increase in the phase volume of the peripheral cytoplasm (up to $\Delta W_{01} = 1.3\ \mu m^3$) and the decrease by ≈ 50% of the phase volume of the dense part of the cell. (d) Uniform shapes of the refractivity profiles $h_{A-D}(r)$ reveal a high homogeneity of PHA-stimulated *T* lymphocyte, the absence of asymmetry, and reduction of the nuclear refractivity. The characteristic maximum identified with the contribution of the chondriome is shifted to the periphery of the cytoplasm and could be consistent with the collapse of the chondriome into smaller mitochondria.

Table 2 Phase portrait of a PHA-activated *T* lymphocyte.

Parameter, boundary	0	1	2	3	4	h_{max}
h_i, (nm)	0	50	127	141	—	152
d_i, (μm)	9.8	7.4	6	5.04	—	—
S_i, (μm^2)	75	43	28	20	—	—
W_i, (μm^3)	8.5	7.2	5.2	3.2	—	—
$\Delta S_{i,i+1}$, (μm^2)	32	15	8	—	—	—
$\Delta W_{i,i+1}$, (μm^3)	1.3	2	2	—	—	—
$\langle \Delta n_i \rangle$	≈0.008	0.023	0.0225	0.0153	—	—
$\Delta V_{i,i+1}$, (μm^3)	280	100	44	65	—	—

graph of the function $S(h)$ [Fig. 3(b)]. The total area of the dense part of the cell ($S_2 \approx 28\ \mu m^2$) increased by 13%. The total area of the cell S_0 grew bigger due to the increased cytoplasmic area $\Delta S_{02} \approx 47\ \mu m^2$ compared with $\Delta S_{02} = 16\ \mu m^2$ in the quiescent cell [Fig. 2(b)]. The graph $W(h)$ [Fig. 3(c)] reveals a 4-fold (up to $\Delta W_{01} = 1.3\ \mu m^3$) increase in the phase volume of the peripheral part of the cytoplasm and a decrease down to $W_2 = 5.2\ \mu m^3$ (by ≈50%) of the dense part of the cell.

Comparison of refractivity profiles in Figs. 3(c) and 2(c) revealed that PHA-activated *T* lymphocyte was more homogeneous, the optical asymmetry virtually disappeared, the nuclear refractivity decreased, and the nucleolus became indistinguishable. Less contrasting characteristic maxima were shifted to the cell periphery. This is consistent with the collapse of the chondriome into smaller mitochondria and their subsequent distribution to cell periphery.[15–17] Decondensation of chromatin[15–17] associated with activated gene transcription, can be a major cause for the decreased nuclear phase thickness and refractivity. The values of the nucleus-to-cytoplasm index decreased to $I_V = 22\%$ versus 75% in intact cells; $I_S = 37\%$ (versus 60%), $I_W = 61\%$ (versus 76%).

Table 2 shows the characteristic phase image parameters of PHA-activated *T* lymphocytes. Most parameters changed compared with intact *T* cells (Table 1). These changes were most clearly manifested in the areas and refractivity of organelles. Together with our earlier findings,[7,10,12] the decrease of the refractivity and the phase thickness in micro-objects exposed to a variety of different inhibitors should be considered fairly universal phenomenon. We attributed some of these effects to the changes in the structure of bound water.[7,10,12]

4 Concluding Remarks

The unique features of phase images of individual cells allowed to localize characteristic points in $S(h)$ and $W(h)$ functions and quantitatively determine key physical parameters, that is, phase thickness, phase volume, and area without reference to any optical model. Measurements of these parameters in absolute units, the estimation of OPD with a high precision, the possibility to record dynamic processes, and an enhanced spatial resolution provide valuable information about cellular morphology and physiology. Furthermore, reproducible and reliable results can be obtained with a small number of cells that might be critical for clinical situations.[18] Simultaneous measurement of the phase thickness and the absorption coefficient allowed to obtain the exact values of these parameters in a single erythrocyte.[18] This and other examples[3] to mention a few, show fundamental difference between the interference methods and other techniques based on measurements of physical parameters in relative units. Obtaining statistically meaningful results with these methods frequently makes the experiments laborious and time consuming.

Our major result is the representation of an individual living cell as a physical object by a phase portrait with potentially big (≈20 to 30) number of important parameters including the refractivity of organelles. A simplified spherical model was sufficient as a first approximation for identification of the elements of phase images with the subcellular structures of the *T* lymphocyte and for quantitative evaluation of their refractivity. In turn, the parameters of the phase images allow making the optical model of the cell more accurate.

To our knowledge, the interference methods have not yet been used to analyze morpho-physiological complexity of nucleated cells. This study is the first to utilize the numerical values of the zone parameters in the phase images for characterization of the functional state of individual *T* lymphocytes. The concept of zones is based on a nonobvious assumption that structural elements of cells are characterized by differential refractivity. Further analysis should be focused on the parameters of boundaries between the zones, their widths and slopes. We believe that the parameters of the phase portraits can be used in the design of new biomedical equipment with a high informative potential and suitability for rapid diagnosis.

Acknowledgments

The authors thank I. Vasilenko and her colleagues for providing donor *T* lymphocytes, and L. Kovalchuk for critical discussions. This work was supported by Grant No. 2.1.2/12944 of Ministry of Education and Science of the Russian Federation.

References

1. Y. Park et al., "Metabolic remodeling of the human red blood cell membrane," *Proc. Natl. Acad. Sci. U. S. A.* **107**(4), 1289–1294 (2010).
2. Y. Park et al., "Static and dynamic light scattering of healthy malaria-parasite invaded red blood cells," *J. Biomed. Opt.* **15**(2), 020506 (2010).
3. Y. Park et al., "Refractive index maps and membrane dynamics of human red blood cells parasitized by Plasmodium falciparum," *Proc. Natl. Acad. Sci. U. S. A.* **105**(37), 13730–13753 (2008).
4. B. Rappaz et al., "Erythrocyte volume and refractive index measurement with digital holographic microscope," *Proc. SPIE* **6445**, 644509, (2007).
5. B. Rappaz et al., "Measurements of the integral refractive index and dynamic cell morphometry of living cells with digital holographic microscopy," *Opt. Express* **13**(23), 9361–9373 (2005).
6. G. Popescu, "Quantitative phase imaging of nanoscale cell structure and dynamics," in *Methods in Cell Biology*, B. Jena, Ed., Vol. **90**, pp. 87–115, Elsevier Inc., Amsterdam, (2008).
7. V. Tychinsky, "The metabolic component of cellular refractivity and its importance for optical cytometry," *J. Biophotonics* **2**(8–9), 494–504 (2009).
8. Z. Wang et al., "Tissue refractive index as marker of disease," *J. Biomed. Opt.* **16**(11), 116017 (2011).
9. V. P. Tychinsky and A. N. Tikhonov, "Interference microscopy in cell biophysics. Principles and methodological aspects of coherent phase microscopy," *Cell Biochem. Biophys.* **58**(3), 107–116 (2010).
10. V. P. Tychinsky and A. N. Tikhonov, "Visualization of individual cells and energy-transducing organelles," *Cell Biochem. Biophys.* **58**(3), 117–128 (2010).
11. Z. Wang et al., "Spatial light interference microscopy (SLIM)," *Opt. Express* **19**(2), 1016–1026 (2011).
12. V. P. Tychinsky, "Dynamic phase microscopy: is a "dialog" with the cell possible," *Physics-Uspekhi* **50**(5), 513–528 (2007).
13. V. P. Tychinsky, "Super-resolution and singularities in phase images," *Phys. Uspekhi* **51**(11), 1161–1169 (2008).
14. Y. Hiramoto, S. Shumei, and S. Yoko, "Refractive index of the protoplasm in sea urchin eggs," *Develop. Growth Differ.* **21**(2), 141–153 (1979).
15. V. Manteifel, L. Bakeeva, and T. Karu, "Ultrastructural changes in chondriome of human lymphocytes after irradiation with He-Ne laser: appearance of giant mitochondria," *J. Photochem. Photobiol.* **38**(1), 25–30 (1997).
16. V. M. Manteifel and T. I. Karu, "Loosening of condensed chromatin in human blood lymphocytes exposed to irradiation with a low-energy He-Ne laser," *Izv. Akad. Nauk Ser. Biol.* **36**(6), 654–661 (2009).
17. V. Manteifel and T. Karu, "Ultrastructural changes in chondriome of human lymphocytes after irradiation with He-Ne laser: appearance of giant mitochondria," *J. Photochem. Photobiol.* **38**, 25–30 (1997).
18. M. Mir, K. Tangella, and G. Popescu, "Blood testing at the single cell level using quantitative phase and amplitude microscopy," *Biomed. Opt. Express* **2**(12), 3259–3266 (2011).